Progress in Oceanography 117 (2013) 37–47

Contents lists available at SciVerse ScienceDirect

Progress in Oceanography

journal homepage: www.elsevier.com/locate/pocean

Enhanced nutrient fluxes at the shelf sea seasonal thermocline caused by stratified flow over a bank ☆

Jacqueline F. Tweddle [a,*], Jonathan Sharples [b,c], Matthew R. Palmer [c], Keith Davidson [d], Sharon McNeill [d]

[a] NAFC Marine Centre, Port Arthur, Scalloway ZE1 0UN, UK
[b] School of Environmental Sciences, University of Liverpool, Liverpool L69 3GP, UK
[c] National Oceanography Centre, Joseph Proudman Building, 6 Brownlow Street, Liverpool L3 5DA, UK
[d] Scottish Association for Marine Science, Scottish Marine Institute, Oban PA37 1QA, UK

ARTICLE INFO

Article history:
Available online 27 June 2013

ABSTRACT

Patches of enhanced chlorophyll *a* (*Chl*) concentrations within the thermocline were observed over the slopes of several banks in the Celtic Sea. The turbulent mixing of nutrients from the bottom water into the thermocline was found to be greatly enhanced over the slope of a bank (up to 52 mmol nitrate m^{-2} day^{-1}), compared to over nearby flat seafloor (~2 mmol nitrate m^{-2} day^{-1}). This increased nutrient supply, forced by locally generated lee waves and internal mixing, is greater than nitrate supplies to the productive tidal mixing fronts or to the shelf edge. We hypothesize this nutrient flux promotes an increase in phytoplankton growth in the thermocline over and downstream of shelf sea banks, contributing to the horizontal patchiness in the thermocline *Chl* signal. The persistence of the strong biological response to mixing at the bank, combined with the ubiquity of shelf sea banks, suggests these bathymetric features have wide importance for "new" primary production in shelf seas.

1. Introduction

Annual rates of primary production within the shelf seas are typically 2–5 times greater than rates in the open ocean, with the shelf seas generating 15–30% of total oceanic primary production despite accounting for <10% of the ocean's area (Wollast, 1998). This carbon fixation makes an important contribution to the ocean sink for atmospheric CO_2 (Frankignoulle and Borges, 2001; Chen and Borges, 2009). Shelf sea primary production also supports a food chain including pelagic herbivores, larval fish (Napp et al., 1996), and commercial fisheries (Cushing, 1995) that provides over 90% of the world's fish catches (Pauly et al., 2002).

The distribution of fishing effort across the shelves is far from uniform (e.g. Murawski et al., 2005; Sharples et al., this issue). Patches of high fish concentrations are often associated with topographic features on the seabed (Genin, 2004). Large topographic features can generate residual flows that retain or provide important transport pathways for fish larvae (e.g. Dickey-Collas et al., 1997; Lough and Manning, 2001; Genin, 2004). Our focus in this project is on smaller features on the shelf seabed, typically 10–30 km long and not high enough to broach the seasonal thermocline. These banks, often associated with high fishing vessel activity (Moum and Nash, 2000; Sharples et al., this issue) are too small to generate significant residual flow. Instead they have been found to produce locally high mixing as stratified water moves over the bank leading to lee waves at the thermocline (e.g. Moum and Nash, 2000). In this component of the work we investigate the biogeochemical consequences of high mixing at Jones Bank in the Celtic Sea. One hypothesis of our project identifies the possibility of enhanced nutrient fluxes over a seabed bank leading to enhanced primary production and/or a shift in the phytoplankton community, potentially providing a "bottom-up" explanation for the increased fishing vessel activity observed at the bank. In this paper we quantify the effect of a bank on the vertical fluxes of nutrients across the base of the sub-surface chlorophyll maximum, demonstrating that these relatively small features can have a significant impact on the supply of nutrients to the primary producers within the summer thermocline of seasonally-stratifying shelf seas.

The background oceanography to the Jones Bank region of the Celtic Sea has been described in Sharples et al. (this issue). Briefly, in temperate shelf seas, such as the Celtic Sea, the water column is fully mixed during winter months. Spring stratification by solar heating generates a surface mixed layer with initially high nutrient concentrations and sufficient light to support rapid phytoplankton growth, resulting in a spring diatom bloom (Pingree et al., 1976; Fasham et al., 1983; Fehling et al., 2006). Following rapid depletion of surface layer nutrients by the bloom, surface layer phytoplankton growth through the rest of the spring and summer occurs mainly using regenerated nitrogen and carbon. New production

* Corresponding author. Tel.: +44 01595 772233
E-mail address: jftweddle@gmail.com (J.F. Tweddle).

0079-6611/$ - see front matter © 2013 The Authors. Published by Elsevier Ltd. All rights reserved.
http://dx.doi.org/10.1016/j.pocean.2013.06.018

over the summer occurs at the tidal mixing fronts (Holligan et al., 1984; Horne et al., 1996), the shelf edge (Joint et al., 2001), and within the seasonal thermocline in a sub-surface chlorophyll maximum (SCM) (Richardson et al., 2000; Sharples et al., 2001). An important aspect of phytoplankton production in the SCM is that new production is strongly controlled by the supply of nitrate from the bottom water (King and Devol, 1979; Sharples et al., 2001), so that a measurement of the vertical nitrate flux provides a measure of the potential for new primary production. This nitrate-fuelled new production within the SCM is likely to contribute significantly to the export of carbon attributable to shelf seas (e.g. Tsunogai et al., 1999), with the organic carbon sinking below the thermocline to be remineralised away from immediate access to the atmosphere (e.g. Thomas et al., 2004). It is also thought to provide a vital food source to pelagic heterotrophs following the spring bloom (Richardson et al., 2000).

Regions of steep seabed topography can have a significant influence on the strength of vertical turbulent mixing in the interior of the water column, which will affect the rate of supply of nutrients into the SCM at the thermocline. Over flat regions of shelf sea seabed in summer, shear generated turbulence arising from barotropic tidal current interaction with the sea floor mixes nitrate into the thermocline. Typical vertical nitrate fluxes measured over such regions of the NW European shelf are about 2 mmol m^{-2} day^{-1} (Sharples et al., 2001; Tweddle, 2007; Rippeth et al., 2009). Mixing within the region of the thermocline has also been observed due to periodic wind-driven inertial oscillations (Palmer et al., 2008; Rippeth et al., 2009), with potential short-term (0.5–1 h duration) spikes of nitrate flux 3 or 4 times greater than the daily mean.

In contrast to regions of flat shelf seabed, the steep topography of the shelf edge has been shown to lead to the formation of internal tidal lee waves and turbulence, driving deep nutrients towards the sea surface (Pingree and Mardell, 1981). Vertical nitrate fluxes at the Celtic Sea shelf edge have been observed up to 9 mmol m^{-2} - day^{-1} with significant contrasts between spring and neap tides (Sharples et al., 2007). Internal lee waves and mixing have also been associated with topographic features on the shelf, e.g. at small banks (Nash and Moum, 2001; Dewey et al., 2005) and fjord-like sills (Farmer and Armi, 1999; Inall et al., 2005). Internal hydraulic jumps and lee waves form downstream of the crest in the topography, generating shear and intensifying turbulence within the pycnocline over the slopes of the topographic feature. However, while the biological implications of baroclinic tides and vertical nutrient fluxes have been investigated at the shelf edge (Sharples et al., 2007, 2009; Schafstall et al., 2010), the impacts of physical processes on nutrient fluxes, and hence phytoplankton production, at smaller seabed banks have so far not been demonstrated. The ubiquity of these bathymetric features across the shelf sea (e.g. see bathymetry map in Sharples et al. (2013)) suggests that the local perturbations they make to vertical biogeochemical fluxes could be significant at the scale of the whole shelf.

2. Methods

Between 2nd July and 27th July 2008, the RRS *James Cook* took part in an inter-disciplinary cruise to the Celtic Sea, in order to elucidate shelf sea processes influencing primary production in the region, particularly those processes occurring over seabed banks (Sharples et al., 2013). Satellite imagery over the Celtic Sea (Fig. 1) illustrates the regional warm surface water indicative of thermal stratification in summer. Five 25 h sampling regimes were

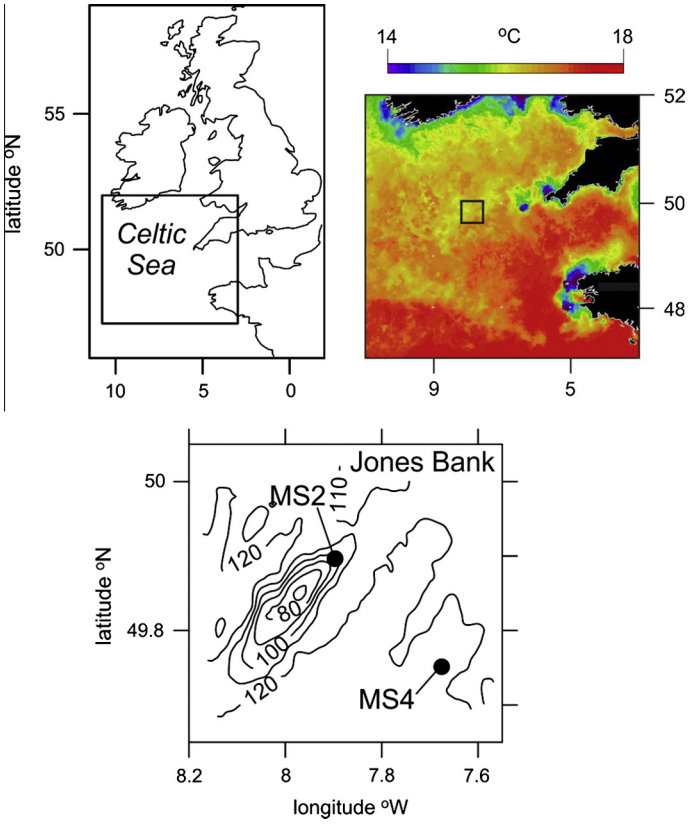

Fig. 1. Location maps for Jones Bank in the Celtic Sea, southwest of the United Kingdom. The satellite image of SST is a 7-day composite of AVHRR data between 21st and 27th July 2008, courtesy of the NERC Earth Observation Data Acquisition and Analysis Service UK. The Bank bathymetry is formed from all of the echosounder data collected during the cruise.

Table 1
Name, position, date, and tidal state of the stations sampled in 2008 in the Celtic Sea.

Station	Location		Date	Yearday	Tide	Winds
MS2a	49.897°N–7.876°E	On Bank	06/07/08	188	Spring	W'ly 25 knots
MS2b	49.897°N–7.876°E	On Bank	14/07/08	196	Neap	W'ly 5–10 knots
MS2c	49.897°N–7.876°E	On Bank	21/07/08	203	Spring	NW'ly 5–10 knots
MS4a	49.750°N–7.667°E	Off Bank	12/07/08	194	Neap	NW'ly 5–10 knots
MS4b	49.750°N–7.667°E	Off Bank	22/07/08	204	Spring	<5 knots

carried out at two sampling sites on and adjacent to Jones Bank (Fig. 1, Table 1), during various times in the spring–neap tidal cycle. Site MS2, occupied three times, was situated over a slope of Jones Bank, and site MS4, occupied twice, was situated over a flat seafloor to the southeast. This bank was chosen because of its simple bathymetry and relative isolation from other banks in the area.

A Rockland Scientific VMP750 vertical microstructure profiler was deployed almost continuously during site occupations. The VMP750 is powered through a cable tether, and so profiles could be taken approximately every 6 min without break, with 3 min free-fall to the seafloor, and 3 min recovering the VMP750 to the ship. The VMP750 profiles between ~8 m below the sea surface (removing ship generated turbulence) to within 15 cm of the seafloor, free-falling with a speed of ~0.7 m s^{-1}. During descent the instrument records pressure, shear, temperature, and conductivity. Turbulent dissipation, ε ($m^2\ s^{-3}$), was calculated with a vertical resolution of 1 m through the water column from the shear data within each of a series of 1 m bins (Dewey et al., 1987; Rippeth et al., 2003). Profiles of vertical turbulent diffusion, K_z, were calculated by (Osborn 1980)

$$K_z = \Gamma \frac{\varepsilon}{N^2} \quad (m^2\ s^{-1}) \tag{1}$$

Here Γ, the mixing efficiency, is considered constant at 0.2. The buoyancy frequency, N (s^{-1}), was calculated by utilizing the density profile measured by the VMP:

$$N^2 = -\frac{g}{\rho}\left(\frac{\partial \rho}{\partial z}\right) \ (s^{-2}) \tag{2}$$

where $g = 9.81$ m s^{-2}, ρ is density, and z is depth (metres, positive upward). For all K_z calculations the buoyancy frequency was calculated over the same depth intervals used for the dissipation measurements. The errors associated with ε and K_z vary, but are at a maximum of 50% at low values ($\varepsilon \sim 10^{-9}\ m^2\ s^{-3}$, Dewey et al., 1987). The VMP750 also recorded chlorophyll fluorescence using a Wetlabs ECO fluorometer.

During each site occupation a Seabird 911 Conductivity-Temperature-Depth sensor (CTD) and rosette package was deployed, on average every 7 h, to obtain profiles of temperature, salinity, and density. Profiles of chlorophyll fluorescence were measured using a Chelsea Instruments Aquatracka MKIII fluorometer attached to the CTD. The CTD was lowered at a rate of 0.5 m s^{-1}, sampling at 24 Hz. CTD temperature errors were of the order of ±0.002 °C, based on pre-cruise and post-cruise laboratory calibrations. CTD salinity uncertainty was ±0.004 (PSS), based on salinity samples analyzed against standard seawater on a Guildline Autosal.

Water samples, taken at several depths through the water column during each CTD cast, were analysed for inorganic nutrient concentrations, and chlorophyll *a* (*Chl*) concentrations. Nutrient samples were analyzed onboard ship for nitrate (NO_3^-) plus nitrite (NO_2^-), ammonium (NH_4^+), silicate (SiO_2), and phosphate (PO_4^-) on a Lachat Autoanalyser using standard AA_II methods (Davidson et al., 2007). The measurement error, based on replicate analysis, was ±5%. *Chl* concentrations were analysed on a Turner Designs Trilogy fluorometer, after sequential filtering of a 500 ml sample water though 20 μm and 2 μm pore size polycarbonate membrane filters. Chlorophyll fluorescence from the fluorometers on the CTD and VMP were calibrated to concentrations of *Chl* using the summed 20 μm and 2 μm results from each sample bottle, with an uncertainty of ±0.03 mg m^{-3}.

A vertical, turbulence driven, flux of a scalar property can be calculated by (e.g. Sharples et al., 2001):

$$flux_{\text{scalar}} = -K_z\left(\frac{\Delta \text{scalar}}{\Delta z}\right) \tag{3}$$

Eq. (3) was used to calculate $flux_{nutrient}$ for each of nitrate (plus nitrite), silicate and phosphate between the bottom mixed layer and the base of the SCM within the thermocline. CTD and VMP750 sampling strategy was based on our previous experience in the region, designed to minimise interruptions to the turbulence time series (Sharples et al., 2001, 2007). We have found that nutrients tend to have robust linear relationships with water density (or temperature) through the base of the thermocline. These relationships allow the nutrient gradients to be calculated using the VMP750 temperature data, thus co-locating the gradient measurement and the estimate of K_z. The nutrient-temperature relationships do not change significantly over the time of a station occupation, reducing the need for frequent CTD and nutrient profiles. The emphasis was instead placed on a few CTD profiles with bottle sampling very well resolved through the thermocline. This has the advantage of allowing more time to be spent profiling with the VMP750, reducing the chances of missing short-lived turbulence events that could be important in affecting the daily flux of a scalar. Nutrient fluxes were taken to be the average of $flux_{nutrient}$, $\overline{-K_z(\frac{\Delta nutrient}{\Delta z})}$, within a 0.5 °C temperature range about an isotherm in the base of the thermocline. Calculating fluxes on an isotherm allows for vertical displacements of the thermocline with respect to depth due to internal waves. The temperature range of 0.5 °C was chosen as a realistic vertical scale over which both K_z and $\Delta nutrient/\Delta z$ were physically resolvable and biologically relevant. For each station all nutrient and temperature data were used to determine the extent of the nutricline, with the temperature at base of the nutricline identified and used as the lower limit to the 0.5 °C range over which the nutrient flux was averaged.

Throughout this paper, significance in statistical tests was taken at the 95% confidence level (i.e. $p < 0.05$).

3. Results

A section undertaken with the towed, undulating CTD package Scanfish along Jones Bank illustrates the bottom and surface mixed layers (BML and SML, respectively), separated by a thermocline (Fig. 2). The section shows the layer of chlorophyll (the SCM) within the lower half of the thermocline (Fig. 2a). Chlorophyll was generally high within the SCM along the entire section, not showing the distinctive maxima over the bank slopes identified in earlier surveys (Sharples et al., 2013). Both temperature and chlorophyll within the BML over the bank were elevated compared to away from the bank, indicating likely recent mixing of water from the base of the thermocline into the BML (Fig. 2b).

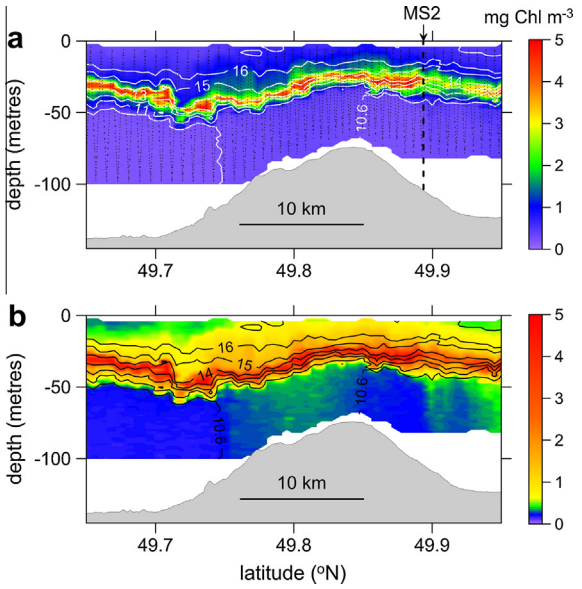

Fig. 2. Transect of temperature and chlorophyll concentrations along the major axis of Jones Bank. Line contours show temperature, colour contours show Chl concentration (mg m^{-3}). (a) and (b) show the same data, but the chlorophyll scale is skewed in (b) to highlight low chlorophyll concentrations in the bottom layer. The Scanfish path is marked in (a), with a dot every 3 data points.

Site MS2 was located over the northeast slope of Jones Bank in ~120 m depth of water, and site MS4 was situated over a region of flat seafloor 25 km southeast of the bank with depth of ~132 m (Fig. 1, Table 1). The sampling during the first occupation of site MS2 (station MS2a) was influenced by gale force winds. This provided an opportunity to compare nutrient supply to the SCM over the bank under conditions of a stormy spring tide (MS2a), a windy neap tide (MS2b) and a spring tide with little wind (MS2c). Away from the bank, site MS4 was occupied during a windy neap tide (MS4a) and quiet spring tide (MS4b).

During all site occupations bottom and surface mixed layers were observed, with SML temperature typically ~4 °C warmer than the BML. Density was primarily controlled by temperature during all stations ($r^2 > 0.999$, $p < 0.05$). The width of the thermocline averaged 20 m during all stations, with the exception of stormy MS2a, where thermocline thickness averaged 30 m. *Chl* concentrations peaked in a sub-surface chlorophyll maximum located towards the base of the thermocline during all stations (Fig. 3). The increased chlorophyll concentration within this layer was attributed mainly to *Phaeocystis* sp. (Davidson et al., 2013).

Inorganic nutrients had highest concentrations in the BML, with nitrate concentrations of ~10.6 mmol m^{-3}, silicate concentrations ~3.0 mmol m^{-3}, and phosphate concentrations of ~0.6 mmol m^{-3}. Nutrient concentrations in the SML were low during all stations (Fig. 3). This region of low nutrient concentration extended down into the top half of the thermocline. Using data from CTD and bottle samples within the base of the thermocline collected during all station occupations, a linear regression provided a relationship between temperature and nitrate ($r^2 = 0.91$, $p < 0.05$, error 16%), silicate ($r^2 = 0.88$, $p < 0.05$, error 20%) and phosphate ($r^2 = 0.85$, $p < 0.05$, error 16%, Fig. 4). These relationships were applied to the VMP750 temperature data within the base of the thermocline. The strength of the nutracline, $\Delta nutrient/\Delta z$, was calculated for each of the nutrients, for each VMP750 profile, and a daily average for each station calculated (Table 2). Gradients of all nutrients varied over the 25 h sampling periods by up to an order of magnitude (data not shown). Comparing the station means in Table 2, the lowest nutrient gradients were seen at MS2 and MS4 during and immediately after the strong winds.

The thermocline, and hence the SCM, underwent vertical displacements during all station occupations (Fig. 5). During neap tide a semi-diurnal (M_2) internal tide dominated the internal wave signal over Jones Bank (MS2b, Fig. 5b). Higher frequency internal waves, with displacements of up to 30 m, were also observed over the bank, particularly during the calm spring tide (MS2c, Fig. 5c, see also Palmer et al., 2013). Away from the bank, at MS4, much weaker vertical movement of the thermocline was observed, with vertical displacements of typically ~5 m (Fig. 5d, e), though with the exception of one 30 m displacement during spring tide (~year-day 204.08, Fig. 5e).

Strongest rates of turbulent dissipation, ε, were seen at the surface and base of the water column during all stations (Figs. 5 and 6). Surface turbulence, caused by wind and wave action, penetrated the full depth of the SML but did not penetrate far into the

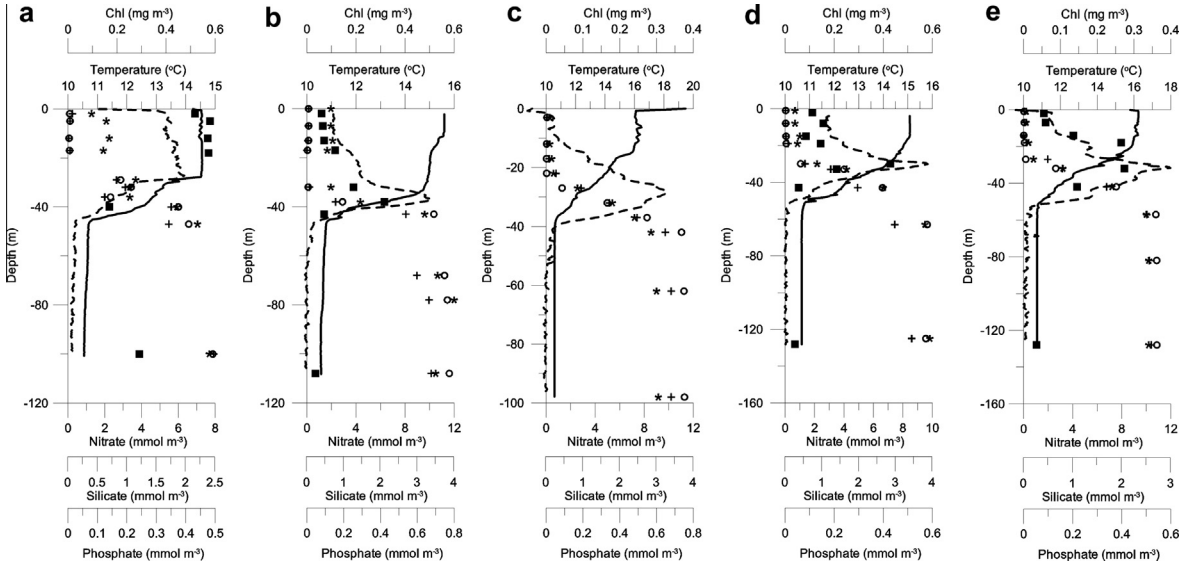

Fig. 3. Example CTD cast data from (a) MS2a (04:00 h UTC 7 July 2008, Yearday 189.1667), (b) MS2b (04:00 h UTC 15 July 2008, Yearday 197.1667), (c) MS2c (14:00 h UTC 21 July 2008, Yearday 203.5833), (d) MS4a (05:00 h UTC 13 July 2008, Yearday 195.2083), and (e) MS4b (04:00 h UTC 23 July 2008, Yearday 205.1667). Solid line represents CTD temperature (°C), broken line CTD Chl *a* concentrations (mg m^{-3}), filled squares Chl a concentrations (mg m^{-3}), open circles nitrate concentrations (mmol m^{-3}), crosses silicate concentrations (mmol m^{-3}), and stars phosphate concentrations (mmol m^{-3}) from rosette bottle sampled water.

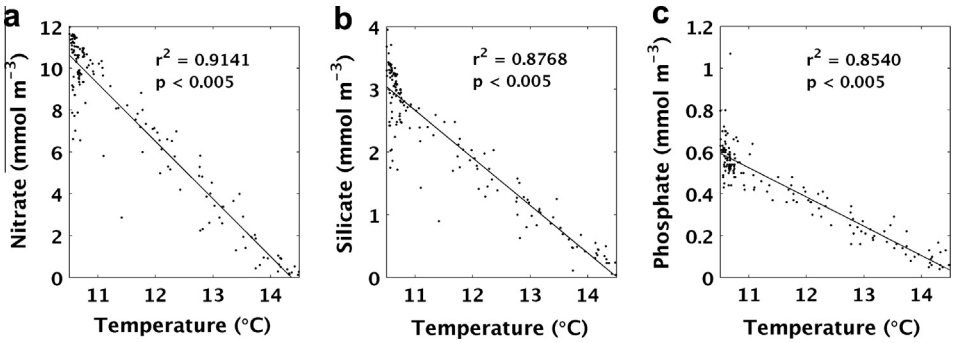

Fig. 4. CTD temperature (°C) and (a) nitrate (mmol m^{-3}), (b) silicate (mmol m^{-3}), and (c) phosphate (mmol m^{-3}) concentrations, from rosette bottle sampled water, were significantly inversely related. Water sample data (dots) plotted from all stations, solid line represents best-fit linear regression, r^2 and p-values as stated on graph.

Table 2
Daily mean vertical nutrient fluxes between the bottom mixed layer and the thermocline ($flux_{nutrient}$, Eq. (3)), and associated daily mean nutrient gradient ($\Delta nutrient/\Delta z$), for nitrate, silicate, phosphate and carbon, and turbulent dissipation (ε_{THERMO}) and vertical diffusivity ($K_{z:THERMO}$) within the base of the thermocline, for Celtic Sea stations sampled during 2008. Values are stated as a daily mean, and the 95% confidence interval of the daily mean in brackets.

Station	$\Delta nitrate/\Delta z$ (mmol m^{-4})	$\Delta silicate/\Delta z$ (mmol m^{-4})	$\Delta phosphate/\Delta z$ (mmol m^{-4})	ε_{THERMO} (m^2 s^{-3})	$K_{z:THERMO}$ (m^2 s^{-1})	$Flux_{nitrate}$ (mmol m^{-2} day)	$Flux_{silicate}$ (mmol m^{-2} day)	$Flux_{phosphate}$ (mmol m^{-2} day)
MS2a	−0.17 (−0.14 to −0.19)	−0.05 (−0.04 to −0.05)	−0.008 (−0.007 to 0.01)	6.9×10^{-5} ($3.7–10.8 \times 10^{-5}$)	2.9×10^{-3} ($1.2–5.1 \times 10^{-3}$)	8.1 (1.0–16.9)	2.2 (0.2–4.6)	0.4 (0.06–0.9)
MS2b	−0.27 (−0.22 to −0.31)	−0.07 (−0.06 to −0.08)	−0.014 (−0.012 to 0.016)	2.3×10^{-6} ($1.5–3.4 \times 10^{-6}$)	3.7×10^{-5} ($0.7–9.5 \times 10^{-5}$)	0.8 (0.1–2.5)	0.2 (0.02–0.7)	0.04 (0.00–0.1)
MS2c	−0.58 (−0.53 to −0.62)	−0.16 (−0.15 to −0.17)	−0.029 (−0.027 to −0.032)	4.9×10^{-5} ($2.5–9.4 \times 10^{-5}$)	1.4×10^{-3} ($0.13–4.5 \times 10^{-3}$)	52 (4–176)	14.2 (1.1–47.8)	2.6 (0.2–9.0)
MS4a	−0.2 (−0.19 to −0.21)	−0.06 (−0.05 to −0.06)	−0.010 (−0.010 to −0.011)	8.5×10^{-6} ($3.9–14.5 \times 10^{-6}$)	2.0×10^{-4} ($3.9–4.6 \times 10^{-5}$)	1.9 (0.3–4.3)	0.5 (0.1–1.2)	0.1 (0.02–0.2)
MS4b	−0.4 (−0.34 to −0.44)	−0.1 (−0.09 to −0.12)	−0.020 (−0.018 to −0.022)	7.9×10^{-6} ($5.3–10.1 \times 10^{-6}$)	7.9×10^{-5} ($1.9–16.0 \times 10^{-5}$)	1.8 (0.4–4.0)	0.5 (0.1–1.2)	0.1 (0.02–0.2)

thermocline. All site occupations exhibited a clear semi-diurnal signal in tidal current velocity, seen in both vessel-mounted and moored ADCPs. Both on and off the bank quarter-diurnal signals in ε were observed close to the bed, with increased values associated with maximum near bed current velocities (Fig. 5, Palmer et al., 2013). Examination of individual VMP profiles revealed the quarter-diurnal intensified turbulent dissipation signal reached maximum heights off the bed of ~60 m during spring tides, ~25 m during neap, with a lag between maximum near bed ε and ε higher in the water column due to vertical change in the region of maximum shear (Simpson et al., 2000). During all site occupations, increased ε was observed within the thermocline, not driven by surface or bed processes, but associated with periods of change in thermocline depth (Fig. 5). Daily mean values of ε at the base of the thermocline (ε_{THERMO}, Table 2) demonstrate the increased rates of turbulent dissipation observed over the bank at spring tides, with higher internal wave activity, compared to neap tides and compared to away from the bank.

Vertical diffusivity, K_z, was calculated from ε, using Eq. (2). All five stations displayed minimum turbulent dissipation in the interior of the water column, and minimum vertical diffusivity, K_z, within the thermocline (Figs. 6 and 7), although care must be taken in interpreting K_z away from the thermocline, where stratification, and hence N^2 (Eq. (2)), was low. K_z within the base of the thermocline, $K_{z:THERMO}$, was calculated within the temperature brackets shown in Fig. 5. $K_{z:THERMO}$, relevant for driving nutrients into the SCM (Eq. (3)), was highly variable both temporally at individual stations and between stations.

$K_{z:THERMO}$ observed during the storm (MS2a, Fig. 7a) was significantly higher than $K_{z:THERMO}$ measured during either the neap tide bank station (MS2b, Fig. 7b) or away from the bank (MS4a and MS4b, Fig. 7d, e respectively), as shown in the daily mean values (Table 2). There was no significant difference in $K_{z:THERMO}$ over the bank between the period of stormy weather and calmer winds at spring tides (MS2a and MS2c, Fig. 7a, c respectively, Table 2). Over the bank at spring tides, episodic increases in $K_{z:THERMO}$ occurred during semi-diurnal mixing events, associated with increased ε (Figs. 5 and 7) which peaked at ~yearday 188.81 (Figs. 5a and 7a), and ~yeardays 203.36, 203.88 and 204.36 (Figs. 5c and 7c). These mixing events were concurrent with vertical movements of the thermocline, and corresponded to times of peak tidal velocities along the bank from southwest to northeast, i.e. over the crest of the bank, towards station MS2.

Away from the bank there was no significant difference in $K_{z:THERMO}$ between neap and spring tides (MS4a and MS4b, Fig. 7d, e respectively, Table 2). $K_{z:THERMO}$ during neap tide stations, on and off the bank (MS2b and MS4a, Fig. 7b, d), were also not of significantly different magnitude (Table 2). Increased mixing events apparently not associated with the barotropic tide were observed during both neap tide stations, at ~yearday 196.63 over the bank (MS2b, Fig. 7b) and at ~yearday 194.60 (MS4a, Fig. 7d) off the bank.

Fluxes of nitrate, silicate and phosphate from the BML into the SCM were calculated (Eq. (3)) for all VMP750 profiles, at all stations. Fluxes of the different nutrients all showed the same pattern, differing only in magnitude (Fig. 8), due to the strong co-variance of the nutrient gradients arising from the common correspondence with temperature in the thermocline. Hence, results are presented here focusing on the nitrate flux.

Temporal variability in nitrate flux was significantly related to variability in $K_{z:THERMO}$ during all stations, with higher vertical fluxes occurring at times of increased vertical diffusivity (Figs. 7

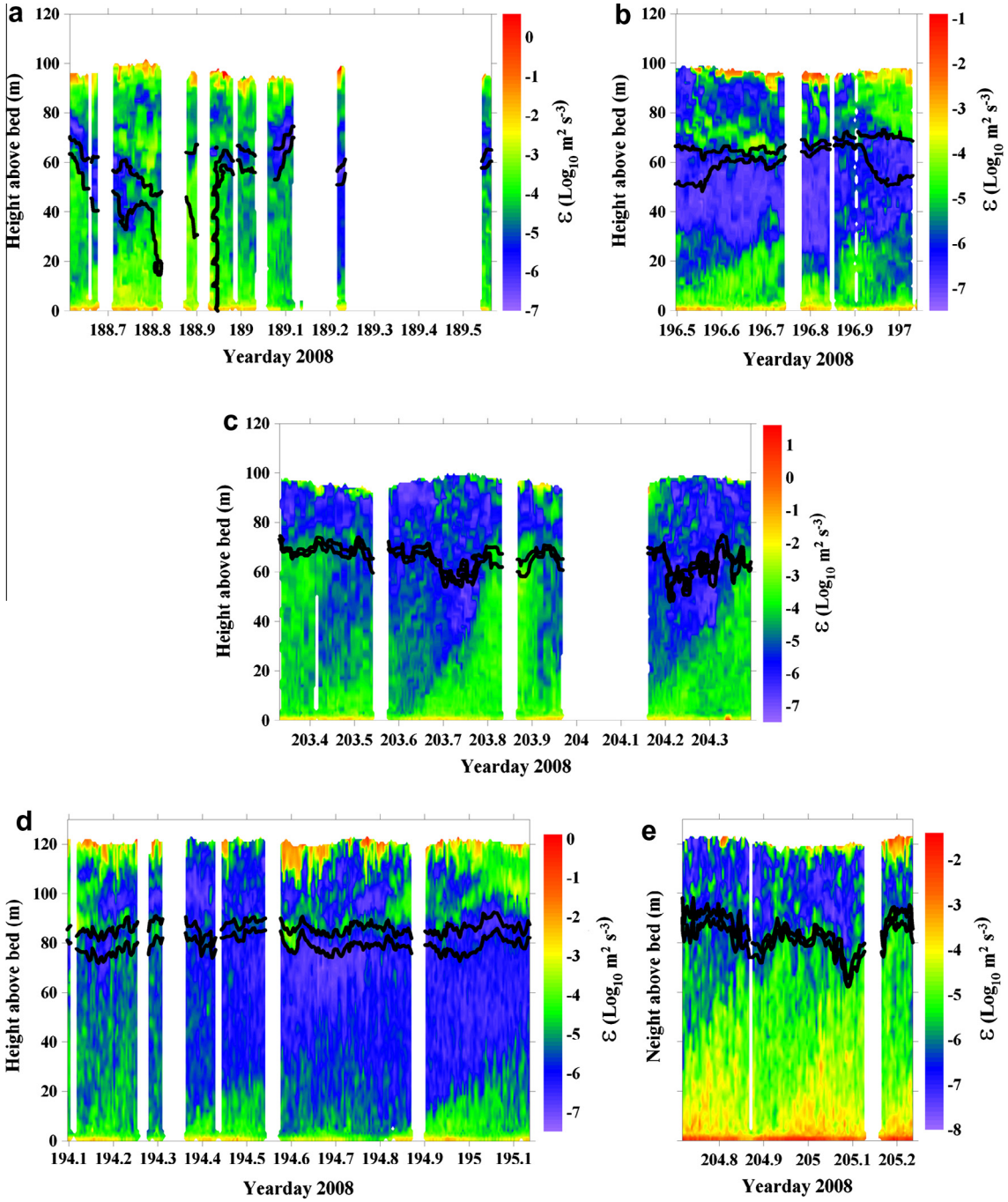

Fig. 5. Contoured time series of turbulent dissipation (ε, $m^2\ s^{-3}$) over the bank at MS2, during windy spring (a, MS2a), neap (b, MS2b), and calm spring (c, MS2c) tides, and away from the bank at MS4, during neap (d, MS4a) and calm spring (e, MS4b) tides. The black solid lines show the temperature bracket over which the fluxes were calculated. Daily average values of ε within this bracket are presented in Table 2.

and 9). The strength of this relationship changed between tidal states, and on and off the bank. Over the bank 34–99.7% of flux variability (Fig. 9a, b, c) was attributable to variability in K_z ($r^2 = 0.34$, $r^2 = 0.996$, and $r^2 = 0.997$ for MS2a, MS2b and MS2c, respectively, $p < 0.05$ for all). Off the bank 69–78% of flux variability in (Fig. 9d, e) was explained by changes in K_z ($r^2 = 0.69$ for MS4a, $r^2 = 0.78$ for MS4b, $p < 0.05$). There was no significant relationship between variability of $flux_{nutrient}$ and $\Delta nutrient/\Delta z$, for nitrate, silicate, or phosphate during any station.

Nutrient fluxes were significantly increased over the bank during the gale force winds (MS2a) compared to neap tide on the bank (MS2b), and compared to off the bank (MS4) at any tidal state (Fig. 9). The daily mean nutrient flux estimates are highest for the calm spring station, MS2c (Table 2), however most of the time series of the nutrient flux is not significantly different than any of the other stations. The high daily mean was greatly influenced by a few, very large pulses of nutrients into the SCM. Particularly strong pulses occurred at ~yeardays 203.36, 203.88 and 204.36 (Fig. 9c), coincident with observed increases in $K_{z:THERMO}$ (Fig. 7c). Off the bank there were no significant differences between the time series of nutrient fluxes observed at neap tide and spring tide (Fig. 9d and e), which is reflected in the daily mean flux estimates (Table 2).

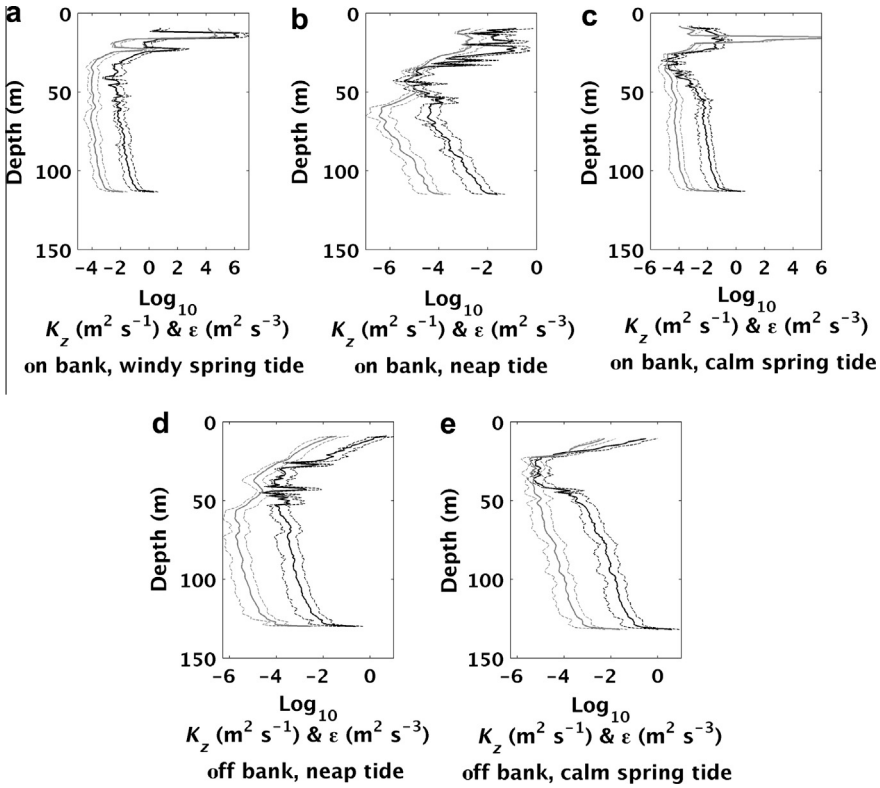

Fig. 6. Daily mean profiles of turbulent dissipation rates (ε, W m^{-3}, solid grey line) and vertical diffusivity (K_z, m^2 s^{-1}, solid black line) profiles over the bank during windy spring (a, MS2a), neap (b, MS2b) and calm spring (c, MS2c) tides, and off the bank during neap (d, MS4a) and calm spring (e, MS4b) tides. Dashed lines represent 95% confidence intervals, calculated using bootstrapping (Efron and Gong, 1983). Note differing *x*-axis scales.

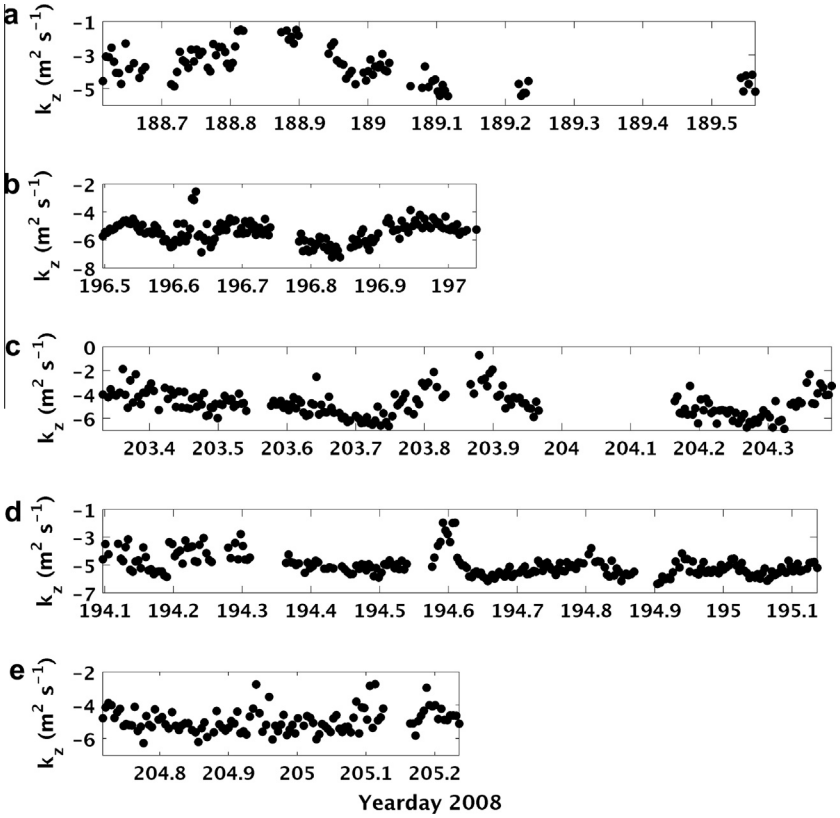

Fig. 7. Time series of $K_{z:THERMO}$ observed over the bank at MS2, during windy spring (a, MS2a), neap (b, MS2b), and calm spring (c, MS2c) tides, and away from the bank at MS4, during neap (d, MS4a) and calm spring (e, MS4b) tides Daily average values of $K_{z:THERMO}$ are presented in Table 2.

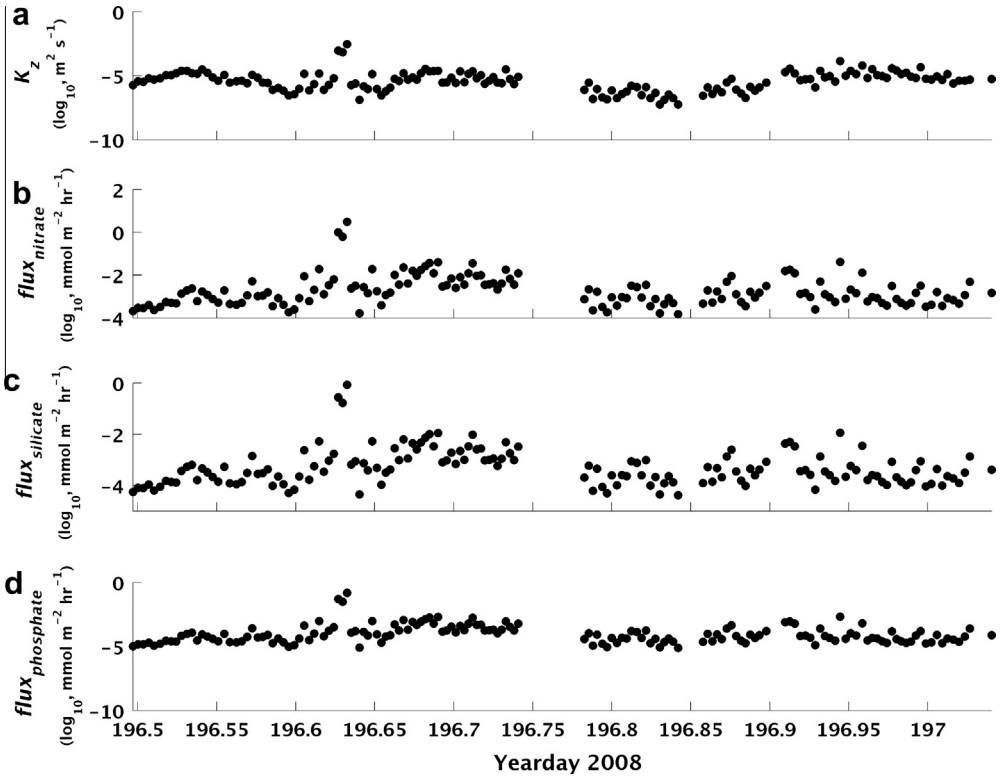

Fig. 8. Time series of a) $K_{z:THERMO}$ and nutrient fluxes (b, $flux_{nitrate}$, c, $flux_{silicate}$ and d, $flux_{phosphate}$) observed over Jones Bank at neap tide, during station MS2b. $flux_{nutrient}$ all co-vary together, and variability is significantly related to $K_{z:THERMO}$ ($r^2 = 0.996$, $p < 0.05$).

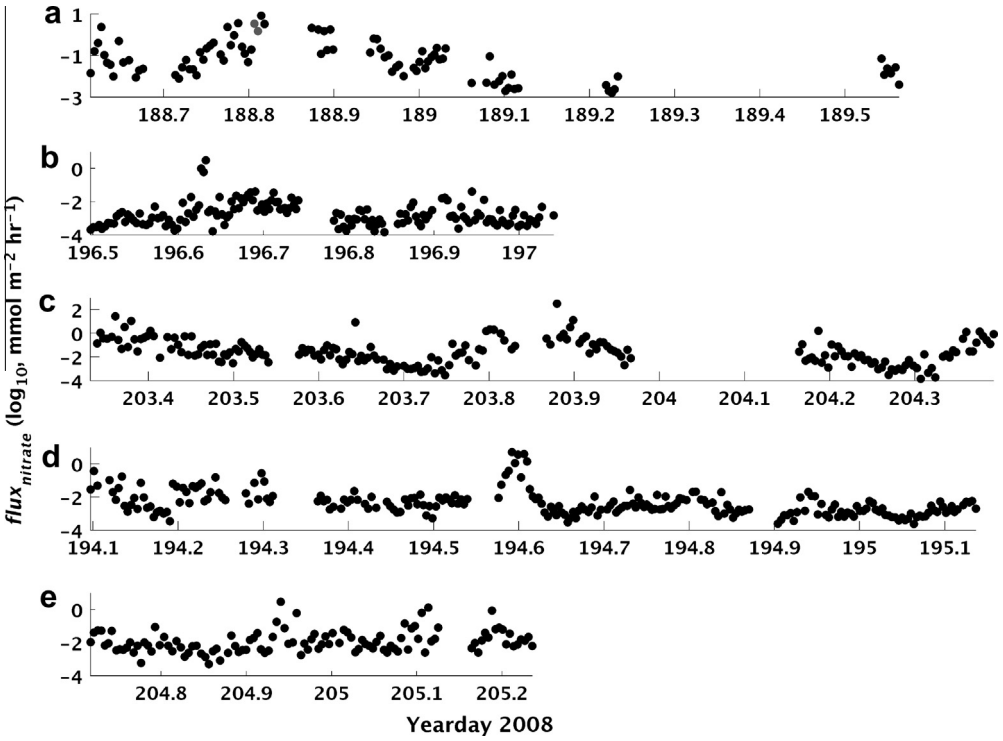

Fig. 9. Vertical nitrate fluxes into the subsurface chlorophyll maximum at stations MS2a (a), MS2b (b), MS2c (c), MS4a (d) and MS4b (e). Filled circles represent estimates for each VMP cast. Upwards fluxes, from the BML into the SCM, are in black. Downward fluxes, from the SCM into the BML, are in red. Daily average values of $flux_{nitrate}$, and $flux_{silicate}$ and $flux_{phosphate}$, are presented in Table 2.

4. Discussion

Mixing events of enhanced turbulent dissipation and vertical diffusivity were observed over the bank during spring tides, associated with periods of internal wave activity. These events drive increased fluxes of nutrients from the BML into the thermocline. Here we will discuss the cause of these mixing events, and further look at the potential influence on primary production, through the impact of the mixing events on nutrient fluxes.

4.1. Influence of the bank on nutrient fluxes

The data from the MS2 site demonstrates enhanced mixing over the bank. Increased internal wave activity was seen, particularly during spring tides, caused by hydraulic control of tidal flow over the bank (Palmer et al., 2013). These regions of hydraulic control create lee waves which, when released by reduction in the tidal currents, propagate as internal waves over the bank slope. These internal waves result in mixing events, which are observed as a short-lived peaks in $K_{z:THERMO}$, occurring with semi-diurnal frequency at spring tides (Fig. 4). These peaks in $K_{z:THERMO}$ drive peaks in $flux_{nutrient}$, pumping nutrients from the BML into the region of the SCM. This leads to the significantly higher nutrient fluxes observed at spring tides compared to neap tides over the bank (Table 2).

Although these lee wave driven mixing events are relatively brief, they have a considerable impact on the daily mean flux estimates. Daily average $flux_{nitrate}$ values can be re-estimated without these events for stations MS2a and MS2c, where internal waves were observed. Without lee wave events the daily mean $flux_{nitrate}$ decreases significantly, from 8.1 to 2.3 mmol m^{-2} day^{-1} during stormy MS2a, and from 52 to 0.8 mmol m^{-2} day^{-1} during the calm spring tide MS2c. This 'background' $flux_{nitrate}$ value for MS2c is very similar to that of MS2b, observed during neap tide and with little internal wave activity, and to those flux values observed at MS4, away from the bank. Thus without these short-lived mixing events the daily supply of nitrate over the bank at spring tide would not be significantly different to the oft reported 'flat seabed' nitrate flux value of ~2 mmol m^{-2} day^{-1} (Sharples et al., 2001; Tweddle, 2007; Rippeth et al., 2009).

It is noteworthy that the nitrate flux observed during calm spring tides over the bank (station MS2c) was substantially larger than that observed during stormy conditions and spring tides (MS2a). Thermocline turbulent diffusivities were similar; the contrast in the nitrate flux is attributable to differences in the vertical nitrate gradient (Table 2). Thus, perhaps counter-intuitively, it appears that the storm acted to reduce the vertical nitrate flux by reducing the vertical nitrate gradient upon which the lee wave turbulence operated.

The spatial influence of these bank-generated internal waves on turbulent mixing was not established, however it is not likely to be extensive. An ADCP and thermistor chain mooring placed at the base of the bank slope showed greatly decreased internal wave activity and associated mixing 10 km down slope of MS2 (Palmer et al., 2013). The elliptical rotation of tidal currents over banks in the Celtic Sea could potentially trigger lee waves to form over different regions of the bank with varying tidal current directions (Palmer et al., 2013). Site MS4 was 23 km from MS2, in a direction perpendicular to the major tidal axis. MS4 stations showed no evidence of bank generated internal waves reaching them. However, the spatial influence of the bank in directly influencing turbulent mixing does necessarily correspond to the affects on primary production, particularly when advection of mixing-influenced water away from the mixing sites is considered (Inall et al., 2013; Davidson et al., 2013).

At site MS4 several mixing events were observed which were not associated with internal waves (e.g. ~yearday 194.60, Fig. 7d). The thermocline of the Celtic Sea is only marginally stable (Palmer et al., 2008, 2013) and small energy inputs can cause mixing. Wind interaction with the water column produces inertial oscillations, which creates shear across the thermocline and can provide enough energy to cause turbulent mixing (Palmer et al., 2008; Rippeth et al., 2009). Inertial oscillations were observed in the vicinity of Jones Bank (Inall et al., 2013), driving a persistent shear layer at the base of the thermocline (Palmer et al., 2013). The inertial oscillations can interact with the barotropic tidal currents to create "shear-spiking" (Burchard and Rippeth, 2009; Inall et al., 2013), potentially driving observed pulses in nutrient flux.

4.2. Influence of the bank on potential primary production

Measurements of primary production (PP) rates, using ^{14}C incubations, were made over the bank (Davidson et al., 2013). During stormy MS2a PP estimates of ~350 mg C m^{-2} day^{-1}, integrated over the whole water column, were measured. The nitrate supply of 8.1 mmol m^{-2} day^{-1}, however, was capable of supporting 'new' PP of ~640 mg C m^{-2} day^{-1}, assuming the Redfield ratio of 106:16 for phytoplankton C:N. Nitrate and phosphate were supplied at a ratio of ~19:1, close to the Redfield *N*:*P* ratio of 16:1. Silicate was supplied below the Redfield ratio of *Si*:*N*:*P* of 15:16:1, at ~5:16:1, however this should be sufficient for diatom growth (Turner et al., 1998). The nitrate fluxes during the calm spring tide (MS2c) could, assuming Redfield C:N, support new production at a rate of 4 g C m^{-2} d^{-1}. This is in excess of any of the production measurements made during the cruise (Davidson et al., 2013), but is similar to the typical carbon fixation rates of 1–6 g C m^{-2} d^{-1} seen in the Celtic Sea during the spring bloom (Pingree et al., 1976; Rees et al., 1999). PP estimates during MS2b, the calm neap tide station on the bank, were ~300 mg C m^{-2} day^{-1} during MS2b. The nitrate flux of 0.8 mmol m^{-2} day^{-1} was capable of supporting only 63 mg C m^{-2} day^{-1} of new production over the bank during this time. Away from the bank ~150 mg C m^{-2} day^{-1} was supportable by the nitrate flux (1.8–1.9 mmol m^{-2} day^{-1}), compared to the ~340 and ~250 mg C m^{-2} day^{-1}, measured during MS4a and MS4b, respectively.

There are several issues to consider when comparing the measured depth integrated PP to the potential 'new' production supported by the supplied nutrients. Firstly, primary production in the SCM is light limited, with light being typically 5–10% of surface values (Hickman et al., in press), so excess nitrate fluxes (i.e. surplus nitrate beyond that required by the light limited rates of SCM PP) are unlikely to be converted to production in that day, but utilised over the following days. Sharples et al. (2007) found potential for excess nitrate supplied over the shelf break during springs to be utilised over the following few days, maximum *Chl* concentrations occurring ~3.5 days after maximum nitrate fluxes. This nitrate also provides a pool of nutrients available for "luxury" uptake. There is the potential for an analogous effect to also occur over banks, allowing the phytoplankton to utilise the supplied nutrients in the days following large nutrient fluxes, without the need for sudden large increases in primary production rates. Model data in Davidson et al. (2013) showed PP rates increased by up to a factor of 2 over the bank slope, peaking just at the edge of the bank, and then reducing to 'background', non-bank levels 25 km (13 days) downstream of the bank.

Secondly, the Eulerian method used in sampling the stations, combined with the advection of water over the bank (Inall et al., 2013), results in complications in comparing primary production observations with those inferred from the nitrate fluxes. The internal wave driven mixing events are short, sharp events, not fully

represented by a daily average. A 'parcel' of water subjected to mixing will experience nutrient fluxes intensified by several orders of magnitude. This 'parcel' will then be advected away from the sampling site, creating a spatially localised patch of nutrient rich thermocline. The remainder of the time 'background' fluxes of nutrients are experienced over the sampling station. The PP values presented in Davidson et al. (2013) were taken from water samples collected during times of 'background' mixing levels, and so are likely lower than those attainable by phytoplankton exposed to strong nutrient fluxes.

At neap tides over the bank, or at any time away from the bank, the amount of potential nitrate-fuelled new production was always less than the primary production measured. We can interpret the ratio between the predicted and observed production as a minimum value for the ratio between new and regenerated production (the *f*-ratio) within the SCM. For the neap tide at MS2b this yields $f = 63/300 = 0.2$. Away from the bank at MS4 we have $f = 150/340 = 0.4$ and $150/250 = 0.6$. When the production possible in response to the nitrate flux is in excess of the observed primary production, the implication is that the nitrate supply will be used over the next few days as the enriched water drifts away from the bank. In that case it is not possible using our data to make any estimate of the SCM production *f*-ratio, though we expect it to be higher than the background values.

4.3. Conclusions

Previously observed nitrate fluxes of 1–2 mmol m^{-2} day^{-1} into the seasonal thermocline (Sharples et al., 2001; Rippeth et al., 2009), are similar to those reported here away from a seabed bank in the stratified shelf sea, driven by the barotropic tide and near inertial oscillations. Nitrate fluxes of 1–9 mmol m^{-2} day^{-1} have been reported at the shelf edge (Sharples et al., 2007), and 3–11 mmol m^{-2} day^{-1} at a tidal mixing front on Georges Bank (Horne et al., 1996). The elevated, though localised, nitrate fluxes at the shelf edge and the tidal mixing fronts is a key factor in those sites being recognised as important regions of biological productivity in shelf seas. Mean daily vertical nitrate fluxes over the topographic feature Jones Bank (0.8–52 mmol m^{-2} day^{-1}) were increased by up to a factor of 25 compared to over a flat seabed, particularly at spring tide. The high spring tide fluxes are driven by short mixing events as a lee wave breaks over the bank slope.

Nitrate and phosphate were supplied in approximate Redfield ratio ($N{:}P \sim 19{:}1$), and silicate supplied in non-limiting amounts ($Si{:}N{:}P \sim 5{:}16{:}1$). The increased nutrient fluxes over the bank at spring tides were capable of supporting greater primary production rates than were observed: 640–4000 mg C m^{-2} day^{-1}, compared to the directly measured rate of ~350 mg C m^{-2} day^{-1}. We infer this discrepancy to be in part due to the dynamic nature of the mixing environment over the bank. Short-lived, spatially limited mixing events driven by lee wave formation and dispersion, lead to a localised patches of relatively high nutrient thermocline waters. This patch is then advected away from its initial position. In effect the bank will 'shed' a patch for each mixing event, each patch containing nutrients sufficient to support enhanced production over the following few days. This enhanced production driven by the banks could significantly raise the typical estimates of annual primary production rates in shelf seas.

Acknowledgements

Our thanks to the Captain and crew of the RRS *James Cook* (cruise JC025) and the technical staff of the U.K. National Marine Facilities. This study was supported by funding from the NERC Oceans 2025 Programme, and the joint NERC-DEFRA Grant NE/F001983/1.

References

Burchard, H., Rippeth, T.P., 2009. Generation of bulk shear spikes in shallow stratified tidal seas. Journal of Physical Oceanography 39, 969–985.
Chen, C.T.A., Borges, A.V., 2009. Reconciling opposing views on carbon cycling in the coastal ocean: continental shelves as sinks and near-shore ecosystems as sources of atmospheric CO2. Deep-Sea Research II 56, 578–590.
Cushing, D.H., 1995. Population Production and Regulation in the Sea. Cambridge University Press, Cambridge, UK.
Davidson, K., Gilpin, L.C., Hart, M.C., Fouilland, E., Mitchell, E., Calleja, I.A., Laurent, C., Miller, A.E.J., Leakey, R.J.G., 2007. The influence of the balance of inorganic and organic nitrogen on the trophic dynamics of microbial food webs. Limnology and Oceanography 52, 2147–2163.
Davidson, K., Gilpin, L.C., Pete, R., Brennan, D., McNeill, S., Moschonas, G., Sharples, J., 2013. Phytoplankton and bacterial distribution and productivity on and around Jones Bank in the Celtic Sea 117, 48–63.
Dewey, R., Richmond, D., Garrett, C., 2005. Stratified tidal flow over a bump. Journal of Physical Oceanography 35, 1911–1927.
Dewey, R.K., Crawford, W.R., Gargett, A.E., Oakey, N.S., 1987. A microstructure instrument for profiling oceanic turbulence in coastal bottom boundary layers. Journal of Atmospheric and Oceanic Technology 4, 288–297.
Dickey-Collas, M., Brown, J., Fernand, L., Hill, A.E., Horsburgh, K.J., Garvine, R.W., 1997. Does the western Irish Sea gyre influence the distribution of pelagic juvenile fish? Journal of Fish Biology 51, 206–229.
Efron, B., Gong, G., 1983. A leisurely look at the bootstrap, the jack-knife and cross-validation. The American Statistician 37, 36–48.
Farmer, D., Armi, L., 1999. The generation and trapping of solitary waves over topography. Science 283, 188–190.
Fasham, M.R.J., Holligan, P.M., Pugh, P.R., 1983. The spatial and temporal development of the spring phytoplankton bloom in the Celtic Sea, April 1979. Progress in Oceanography 12, 87–145.
Fehling, J., Davidson, K., Bolch, C.J., Tett, P., 2006. Seasonality of Pseudo-nitzschia spp. (Bacillariophyceae) in Scottish waters. Marine Ecology Progress Series 323, 91–105.
Frankignoulle, M., Borges, A.V., 2001. European continental shelf as a significant sink for atmospheric carbon dioxide. Global Biogeochemical Cycles 15, 569–579.
Genin, A., 2004. Bio-physical coupling in the formation of zooplankton and fish aggregations over abrupt topographies. Journal of Marine Systems 50, 3–20.
Hickman, A.E., Moore, C.M., Sharples, J., Lucas, M.I., Tilstone, G.H., Krivtsov, V., Holligan, P.M., in press. Primary production and nitrate uptake within the seasonal thermocline of the Celtic Sea. Marine Ecology Progress Series.
Holligan, P.M., Harris, R.P., Newell, R.C., Harbour, D.S., Head, R.N., Linley, E.A.S., Lucas, M.I., Tranter, P.R.G., Weekley, C.M., 1984. Vertical distribution and partitioning of organic carbon in mixed, frontal and stratified waters of the English Channel. Marine Ecology Progress Series 14, 111–127.
Horne, E.P.W., Loder, J.W., Namie, C.E., Oakey, N.S., 1996. Turbulent dissipation rates and nitrate supply in the upper water column on Georges Bank. Deep-Sea Research II 43, 1683–1712.
Inall, M., Aleynik, D., Neil, C., 2013. Horizontal advection and dispersion in a stratified shelf sea: the role of inertial oscillations 117, 25–36.
Inall, M., Rippeth, T., Griffiths, C., Wiles, P., 2005. Evolution and distribution of TKE production and dissipation within stratified flow over topography. Geophysical Research Letters 32.
Joint, I., Wollast, R., Chou, L., Batten, S., Elskens, M., Edwards, E., Hirst, A., Burkill, P., Groom, S., Gibb, S., Miller, A., Hydes, D., Dehairs, F., Antia, A., Barlow, R., Rees, A., Pomroy, A., Brockmann, U., Cummings, D., Lampitt, R., Loijens, M., Mantoura, F., Miller, P., Raabe, T., Alvarez-Salgado, X., Stelfox, C., Woolfenden, J., 2001. Pelagic production at the Celtic Sea shelf break. Deep-Sea Research Part Ii-Topical Studies in Oceanography 48, 3049–3081.
King, F.D., Devol, A.H., 1979. Estimates of vertical eddy diffusion through the thermocline from phytoplankton nitrate uptake rates in the mixed layer of the eastern tropical Pacific. Limnology and Oceanography 24, 645–651.
Lough, R.G., Manning, J.P., 2001. Tidal-front entrainment and retention of fish larvae on the southern flank of Georges Bank. Deep Sea Research Part II: Topical Studies in Oceanography 48, 631–644.
Moum, J.N., Nash, J.D., 2000. Topographically induced drag and mixing at a small bank on the continental shelf. Journal of Physical Oceanography 30, 2049–2054.
Murawski, S.A., Wigley, S.E., Fogarty, M.J., Rago, P.J., Mountain, D.G., 2005. Effort distribution and catch patterns adjacent to temperate MPAs. Ices Journal of Marine Science 62, 1150–1167.
Napp, J.M., Incze, L.S., Ortner, P.B., Siefert, D.L.W., Britt, L., 1996. The plankton of Shelikof Strait, Alaska: standing stock, production, mesoscale variability and their relevance to larval fish survival. Fisheries Oceanography 5, 19–38.
Nash, J.D., Moum, J.N., 2001. Internal hydraulic flows on the continental shelf: high drag states over a small bank. Journal of Geophysical Research-Oceans 106, 4593–4611.
Osborn, T.R., 1980. Estimates of the local rate of vertical diffusion from dissipation measurements. Journal of Physical Oceanography 10, 83–89.

Palmer, M.R., Inall, M.E., Sharples, J., 2013. The physical oceanography of Jones Bank: a mixing hotspot in the Celtic Sea 17, 9–24.
Palmer, M.R., Rippeth, T.P., Simpson, J.H., 2008. An investigation of internal mixing in a seasonally stratified shelf sea. Journal of Geophysical Research 113.
Pauly, D., Christensen, V., Guénette, S., Pitcher, T.J., Sumaila, U.R., Walters, C.J., Watson, R., Zeller, D., 2002. Towards sustainability in world fisheries. Nature 418, 689–695.
Pingree, R.D., Holligan, P.M., Mardell, G.T., Head, R.N., 1976. The influence of physical stability on spring, summer and autumn phytoplankton blooms in the Celtic Sea. Journal of the Marine Biological Association of the UK 56, 845–873.
Pingree, R.D., Mardell, G.T., 1981. Slope turbulence, internal waves and phytoplankton growth at the Celtic Sea shelf-break. Philosophical Transactions of the Royal Society of London A 302.
Rees, A.P., Joint, I., Donald, K.M., 1999. Early spring bloom phytoplankton-nutrient dynamics at the Celtic Sea Shelf Edge. Deep-Sea Research Part I 46 (3), 483–510.
Richardson, K., Visser, A.W., Pedersen, F.B., 2000. Subsurface phytoplankton blooms fuel pelagic production in the North Sea. Journal of Plankton Research 22, 1663–1671.
Rippeth, T.P., Simpson, J.H., Williams, E., Inall, M.E., 2003. Measurement of the rates of production and dissipation of turbulent kinetic energy in an energetic tidal flow: Red Wharf Bay revisited. Journal of Physical Oceanography 33, 1889–1901.
Rippeth, T.P., Wiles, P., Palmer, M.R., Sharples, J., Tweddle, J.F., 2009. The diapycnal nutrient flux and shear-induced diapycnal mixing in the seasonally stratified western Irish Sea. Continental Shelf Research 29, 1580–1587.
Schafstall, J., Dengler, M., Brandt, P., Bange, H., 2010. Tidal-induced mixing and diapycnal nutrient fluxes in the Mauritanian upwelling region. Journal of Geophysical Research 115.
Sharples, J., Moore, C.M., Hickman, A.E., Holligan, P.M., Tweddle, J.F., Palmer, M.R., Simpson, J.H., 2009. Internal tidal mixing as a control on continental margin ecosystems. Geophysical Research Letters 36.
Sharples, J., Moore, C.M., Rippeth, T.P., Holligan, P.M., Hydes, D.J., Fisher, N.R., Simpson, J.H., 2001. Phytoplankton distribution and survival in the thermocline. Limnology and Oceanology 46, 486–496.
Sharples, J., Palmer, M.R., Ellis, J., Hickman, A.E., Nolan, G., this issue. Internal mixing and the biology of the Celtic Sea in Summer.
Sharples, J., Tweddle, J.F., Green, J.A.M., Palmer, M.R., Kim, Y.N., Hickman, A.E., Holligan, P.M., Moore, C.M., Rippeth, T.P., Simpson, J.H., Krivtsov, V., 2007. Spring-neap modulation of internal tide mixing and vertical nitrate fluxes at a shelf edge in summer. Limnology and Oceanography 52, 1735–1747.
Simpson, J.H., Rippeth, T., Campbell, A.R., 2000. The phase lag of turbulent dissipation in tidal flow. In: Yanagi, T. (Ed.), Interaction between Estuaries, Coastal Seas and Shelf Seas. Terra Scientific, pp. 57–67.
Thomas, H., Bozec, Y., Elkalay, K., de Baar, H.J.W., 2004. Enhanced open ocean storage of CO_2 from shelf sea pumping. Science 304, 1005–1008.
Tsunogai, S., Watanabe, S., Sato, T., 1999. Is there a "continental shelf pump" for the absorption of atmospheric CO_2? Tellus B 51, 701–712.
Turner, R.E., Qureshi, N., Rabalais, N.N., Dortch, Q., Justic, D., Shaw, R.F., Cope, J., 1998. Fluctuating silicate:nitrate ratios and coastal plankton food webs. Proceedings of the National Academy of Sciences of the United States of America 95, 13048–13051.
Tweddle, J.F., 2007. Nutrient Fluxes into the Seasonal Thermocline of the Celtic Sea. School of Ocean and Earth Sciences, vol. Ph.D. Southampton, University of Southampton, p. 243.
Wollast, R., 1998. Evaluation and comparison of the global carbon cycle in the coastal zone and in the open ocean. In: Brink, K., Robinson, A.R. (Eds.), The Sea, vol. 10. Wiley, New York, pp. 213–252.